Non-Iterative Microwave Imaging Solutions for Inverse Problems Using Deep Learning

Thathamkulam A. Anjit[1, *], Ria Benny[1], Philip Cherian[2], and Palayyan Mythili[1]

Abstract—This paper describes a U-net based Deep Learning (DL) approach in combination with Subspace-Based Variational Born Iterative Method (SVBIM) to provide a solution for the quantitative reconstruction of scatterer from the measured scattered field. The proposed technique can be used as an alternative to conventional time consuming and computationally complex iterative methods. This technique comprises a numerical solver (SVBIM) for generating the initial contrast function and a DL network to reconstruct the scatterer profile from the initial contrast function. Further, the proposed technique is validated against theoretical and experimental results available from the literature. Root Mean Square Error (RMSE) value is used as the metric to measure the accuracy of the reconstructed image. The RMSE values of the proposed method show a significant reduction in the reconstruction error compared with the recent Back Propagation-Direct Sampling Method (BP-DSM). The proposed method produces an RMSE value of 0.0813 against 0.1070 in the case of simulation (Austria Profile). The error value obtained by validating against the FoamDielExt experimental database in the case of the proposed method is 0.1037 against 0.1631 reported for BP-DSM method.

1. INTRODUCTION

Microwave Imaging (MWI) is a promising non-contact and non-destructive imaging technique that has been effectively used for a wide range of engineering and medical applications. Major applications which utilize the MWI are surveillance, microwave remote sensing, non-destruction detection, biomedical imaging, and geological exploration [1, 2]. MWI can be broadly classified into two categories, namely quantitative and qualitative methods. Qualitative methods can only retrieve the shape and location of the scatterers within the imaging domain, hence these techniques are used for detection purposes. On the other hand, the quantitative imaging technique is an electromagnetic inverse scattering problem that aims to reconstruct the spatial permittivities of the scatterer from the knowledge of the measured scattered fields with a few receivers [3, 4]. These Inverse Scattering Problem (ISP) techniques are generally slower, ill-posed, and nonlinear. Imaging such a scatterer from the ISP is achieved by solving the Electric Field Integral Equation (EFIE). These EFIE equations are nonlinear with two sets of unknown quantities (a) the dielectric profile and (b) the total electric field inside the scattering object [5]. This non-linearity occurs due to three major limitations (a) presence of evanescent waves — fine-grained details will be lost in the inversion process since the evanescent waves produced in the region under study do not reach the receiver location, (b) local minima — by increasing the number of fields of excitation and the number of sensors, and local minima(s) can be reduced to some extent [6], and (c) sensitivity of the inverse problem to noise — the effect of noise can be reduced by employing a conventional regularization technique along with the inversion algorithm.

Over the past decades, ISP is often formulated as a linear inverse problem by adopting scattering models based on Born iteration method (BIM) and Rytov method which produce iterative solutions to

the problem [7]. These approximations are based on the strength of the scatterer with respect to the propagation medium. Born approximation is the simplest, which assumes that the scattered electric field can be written in terms of the incident field. The Rytov approximation on the other hand is based on the phase of the electromagnetic field. These algorithms are valid only for weak scatterers with low dielectric contrast values. The objects made of high contrast material pose a challenge to conventional methods in terms of accuracy. The high complexity and long computing time makes the solving of the inverse scattering problem a challenge in the case of applications with objects having high contrast profile. Besides, the dependence on the Green's function to construct electromagnetic (EM) coupled equations in conventional methods greatly limits their application in practical complex scenarios, where the Green's function has to be constructed for each iteration.

Deterministic iterative procedures (like Newton and quasi-Newton gradient method, conjugate gradient method (CG), etc.) [8] are commonly used to solve the ill-posed nonlinear problem. The main advantage of the deterministic methods is their faster convergence. As these methods are local search methods, they require a reliable starting point for the solution to converge. The stochastic optimization methods (e.g., genetic algorithm (GA), Particle Swarm Optimization (PSO), differential annealing, Ant Colony Optimizer (ACO)) [9] proceed by constructing a nonlinear cost function relating the measured scattered fields to the permittivity of the unknown scatterer, and then the constructed cost function is minimized. Stochastic algorithms are inherently able to find the global optimal solution from an arbitrary starting point irrespective of the non-linearity and ill-posedness of the problem. This, however, leads to a higher computational cost. Both deterministic and stochastic methods along with a regularization scheme help to reduce the original ill-posed problem by adding some a-priori information about the scatterer. Under certain constraints, an optimal solution can be determined by either minimizing or maximizing the regularized objective function with the trade-off between noise and acquisition time. Short data acquisition time leads to severe degradations of image quality, while long acquisitions may cause motion artifacts.

With the introduction of Compressive Sensing (CS) and the related regularizers (such as Basic pursuit de-noising (BPDN), orthogonal matching pursuit (OMP), and total variation (TV)), some sparseness-aware inverse scattering algorithms were proposed in [10]. These robust and practical algorithms are capable of producing excellent image quality along with reasonable computational complexity. Due to these advantages, the CS techniques have been particularly influential in the field of biomedical imaging, e.g., in Magnetic Resonance Imaging (MRI) [11] and X-ray computed tomography (CT) [12]. Although these methods can produce acceptable results for objects with moderate size and contrast, it remains an outstanding challenge to deploy them in realistic scenarios involving high contrast objects due to the very expensive computational costs. In the implementation stage, CS techniques need more attention in certain areas. CS theory does not always properly exploit all of the a-priori knowledge that is available in imaging applications. Moreover, enforcing Restricted Isometry property (RIP) condition upon scattered data is not a feasible option. Therefore, systems that generate sparse data by avoiding the need to check the RIP of the kernel operator may be adopted to solve this concern [13].

Most recently, methodologies based on the artificial neural network have also been proposed [14] to extract information about the geometry and electromagnetic properties of the scatterer. Since the scatterer is spatially inhomogeneous and the number of scatterers can be arbitrary, most of these deep learning methods use certain parameters such as position, shape, and size to represent the scatterer. More versatile approaches to represent the scatterer are based on the pixel basis, i.e., the value of permittivity of each pixel. In the past few years, deep learning has emerged as one of the most powerful approaches in several areas of regression and classification problems. Researchers have recently proposed Convolutional Neural Network (CNN) to solve the electromagnetic inverse scattering problem, where a set of parameters like geometrical and spatial properties are extracted [15]. CNN deep learning algorithm works with neurons that have learnable weights and biases. They combine the extracted features and aggregate them in a nonlinear fashion to predict the output. Due to the nonlinear fitting ability and single step prediction, deep learning methods have been adopted in real-time quantitative microwave imaging. In [15], the image reconstructed using the back propagation scheme is used to feed the CNN in learning based method. Guo et al. [16] use CNN for nonlinear inversion, where it is used to solve the time consuming gradient in traditional objective function approach. These works have mentioned the
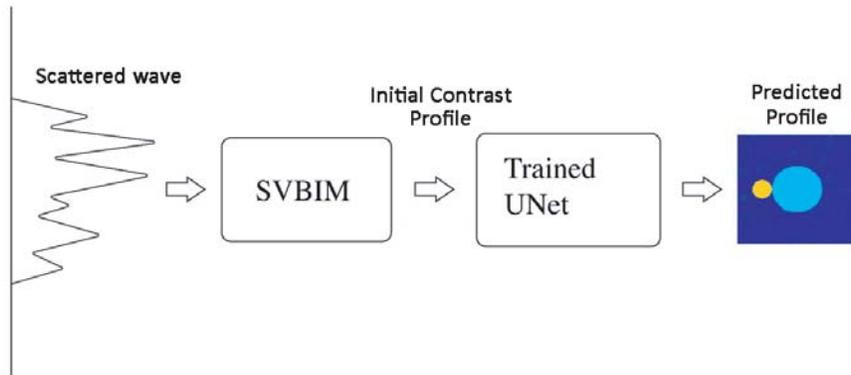
Figure 1. Proposed block diagram for Quantitative Microwave Imaging.

effectiveness of using a learning based method for the effective reconstruction of quantitative MWI.

In this paper, a U-Net based deep learning approach is designed to solve the ISP in combination with the primary results obtained from S-VBIM instead of BIM. The proposed method can provide a robust reconstruction along with a better resolution of the object under consideration compared to existing techniques. The performance of the proposed method has been validated by comparing with the results reported by Zhan et al. (2020) [17]. The paper has been organised as follows. Section 2 describes the linear approximation of the electromagnetic inverse problem using Subspace-based Virtual Born Iteration Method (S-VBIM). Deep learning based approach adopted to solve the inverse problem is explained in Section 3. Section 4 elaborates the dielectric profile reconstruction results obtained using the proposed methodology. In addition, the performance of the method has been validated using an available experimental database [18]. Finally, Section 5 concludes the paper.

2. PROBLEM STATEMENT

This paper investigates a two-dimensional (2D) quantitative approach for reconstructing the scatterer (object function) from the scattered field measured around it. Fig. 1 shows the proposed block diagram of the quantitative approach to retrieve the dielectric parameters of the object function under investigation. The measurement of the scattered field is done using a tomographic arrangement of antennas. By applying S-VBIM, the measured scattered fields are used to generate an initial contrast function. This initial contrast profile is used as the input for the training of the Unet-based deep learning network whose output is the final object profile of the scatterer. Section 2.1 describes the formulation of the forward problem for the accumulation of the scattered signals. Section 2.2 describes the formulation of S-VBIM to generate the initial contrast profile, and Section 2.3 refers to the design of CNN used for predicting the contrast profile.

2.1. Forward Problem

Consider a 2D transverse magnetic (TM, i.e., E_z polarization) inverse scattering problem. The object of interest is embedded in an imaging domain V, which has a complex permittivity varying in the x-y plane. The objective is to image the dielectric permittivity profile of the scatterer from a finite number of scattered data measured around the vicinity of the object under investigation. The tomographic arrangement of the transmitter and receiver antennas for MWI is shown in Fig. 2. The object under investigation is assumed to be inhomogeneous with respect to the dielectric permittivity ϵ_r and conductivity σ. This object is immersed in a homogeneous background medium having a permittivity ϵ_b. The object is illuminated by a TM polarised wave whose magnetic field is transverse to the axis of the scatterer. N_t number of transmitting antennas and N_r number of receiver antennas are positioned around the object at equal angular intervals. The entire arrangement corresponding to Fig. 2 is divided into an object domain, i.e., the area which encloses the object to be imaged and the measurement
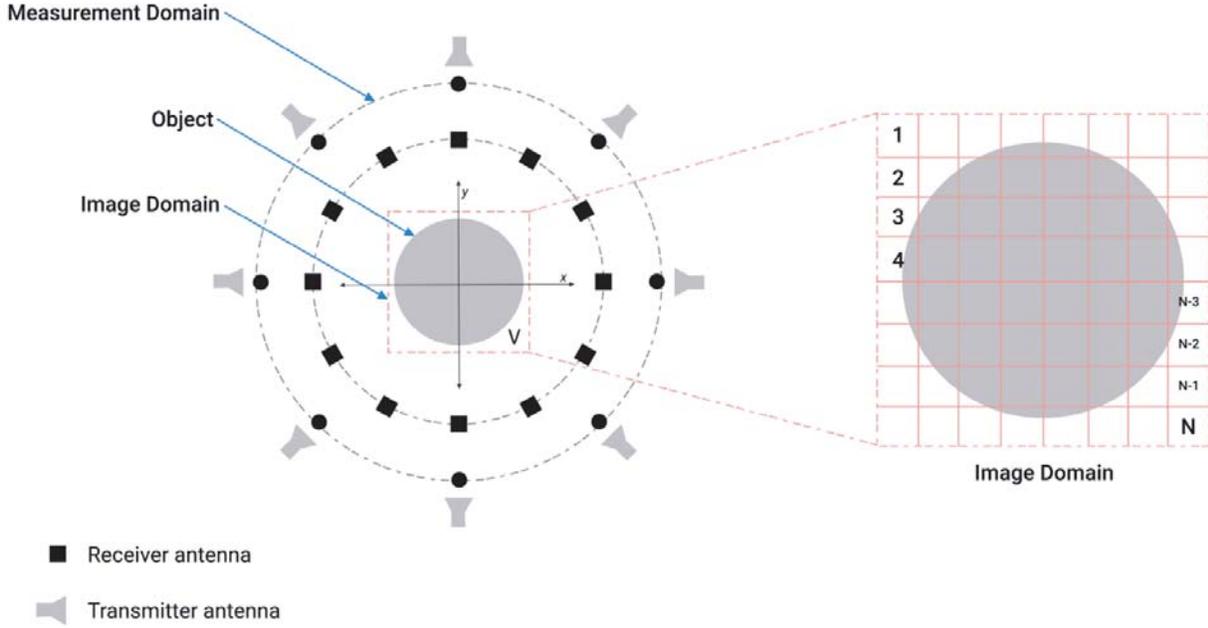
Figure 2. Tomographic arrangement of transmitter and receiver antennas.

domain, where the measurements are done. The object domain is further divided into a grid of square-shaped cells. Within each cell, the total electric field and complex permittivity is assumed to be a constant. The distance to any point inside the object domain is r and to any measurement point in the measurement domain is r' from the origin.

The imaging procedure begins with the illumination of the object under study from multiple angles. The scattered fields for the given scatterer are then obtained at the receivers which are placed at equal intervals. This process is termed as the forward problem. The total electric field in the imaging domain V is expressed by Electric Field Integral Equation (EFIE) as [19]:

$$E_z^{tot}(r) = E_z^{inc}(r) + \int_V g\left(k_0; r, r'\right) [k^2\left(r'\right) - k_0^2\left(r'\right)] E_z^{tot}\left(r'\right) dr' \tag{1}$$

i.e., the total field $E_z^{tot}(r)$ in the imaging domain can be written as the sum of incident field $E_z^{inc}(r)$ and the scattered field. Here, $g(k_0; r, r')$ represents the Green's function of the background medium, where k_0 represents the wavenumber of the background medium, and k represents the wavenumber of the scatterer. The imaging domain is discretized into $N \times N$ square cells. Then, EFIE regarding the above system can be written in matrix form as

$$\overline{E}^{tot} = \overline{E}^{inc} + \overline{G}_V \cdot \overline{\zeta} . \overline{E}^{tot} \tag{2}$$

where $\overline{\zeta}$ is a diagonal matrix which represents the contrast function. The actual scattered field measured at the receiver is written as:

$$\overline{E}^{scat} = \overline{G}_s \cdot \overline{\zeta} \cdot \left(\overline{I} - \overline{G}_V \cdot \overline{\zeta}\right)^{-1} \cdot \overline{E}^{inc} \tag{3}$$

where $\overline{\zeta}$ is the actual dielectric distribution of scatterer.

2.2. Linear Approximation of EM Inverse Scattering Problem with S-VBIM

The reconstruction of the dielectric profile from the measured scattered field data within the imaging domain is a nonlinear and ill-posed problem. A common approach to solve the inverse problem is to rely on iterative inversion algorithms.

Approximations like Born iteration method (BIM) or Distorted Born iterative methods (DBIM) are often used as a counter measure to non-linearity. In the kth iteration, BIM uses an approximation to linearize the equation [19]:

$$\overline{E}_{meas}^{scat} = \overline{G}_s \cdot \overline{\zeta}_k \cdot (\overline{I} - \overline{G}_V \cdot \overline{\zeta}_{k-1})^{-1} \cdot \overline{E}^{inc} \tag{4}$$

where $\overline{E}_{meas}^{scat}$ is the measured scattered field, I the identity matrix, $\overline{G}_s$ the Measurement Greens function, and $\overline{\zeta}_{k-1}$ the reconstructed dielectric profile from the previous iteration step. In VBIM, the variational form of Eq. (4) is used in the inverse problem so that

$$\delta\overline{E}^{scat} = \overline{G}_s \cdot \delta\overline{\zeta}_k \cdot \left(\overline{I} - \overline{G}_V \cdot \overline{\zeta}_{k-1}\right)^{-1} \cdot \overline{E}^{inc} \tag{5}$$

where

$$\delta\overline{E}^{scat} = \overline{E}_{meas}^{scat} - \overline{E}_k^{scat} \tag{6}$$

$$\delta\overline{\zeta} = \overline{\zeta}_k - \overline{\zeta}_{k-1} \tag{7}$$

$\delta\overline{E}^{scat}$ is the difference between the measured value and the computed scattered field in the kth iteration; $\delta\overline{\zeta}$ represents the difference between the kth and $(k-1)$th iteration values of the dielectric profile in the imaging domain. Equation 5 refers to the variation of scattered field caused by the variation of the parameter $\delta\overline{\zeta}_k \cdot (\overline{I} - \overline{G}_D \cdot \overline{\zeta}_{k-1})^{-1} \cdot \overline{E}^{inc}$. This quantity can be considered as the variation of the induced current $\delta\overline{J}$. $\overline{G}_s$ is the mapping function which relates the variation of the induced current in the imaging domain to the variation of the scattered field on the receiver on each receivers. By taking the singular value decomposition of the mapping function, it is rearranged as

$$\overline{G}_s = \sum_i \overline{u}_i \sigma_i \overline{v}_i^* \tag{8}$$

$$\overline{G}_s \cdot \overline{v}_i = \sigma_i \cdot \overline{u}_i as \tag{9}$$

The vector of variational scattered field $\delta\overline{E}^{scat}$ can be represented as a span of the left singular vector $\overline{u}_i$ and the vector of variation of induced current $\delta\overline{J}$ as a span of the right singular vector $\overline{v}_i$. The variational induced current $\delta\overline{J}$ cannot be uniquely determined solely from Eq. (5), since only the radiating part can be obtained accurately. Due to the presence of noise, singular values with smaller magnitude are mostly affected. Hence, implementing this method's singular values is arranged in the decreasing order, such that $\sigma_1 \geq \sigma_2 \geq \ldots \geq \sigma_{L_o} \geq \sigma_{L_0+1} = \sigma_{L_0+2} = \ldots = \sigma_M = 0$. The first L values which are less affected by noise are retained. The rest of the smaller singular values are removed. Choosing the value of L (an integer) is very crucial, because the optimal choice for the number of singular values varies with the signal to noise ratio (SNR) of the measurements and is determined from Morozov's discrepancy principle [20]. In this work, the optimal value for L is chosen as 15 [21].

$$\delta\overline{J}^d = \sum_{i=1}^{L} \frac{\overline{u}_i^* \cdot \delta\overline{E}^{scat}}{\sigma_i} \tag{10}$$

$\delta\overline{J}^d$ is the deterministic part of the variational induced current since it contributes to the most part of the variational scattered field on the receiver.

The exact total electric field is

$$\overline{E}^{tot} = \overline{E}^{inc} + \overline{G}_D \cdot \overline{J} \tag{11}$$

where $\overline{J}$ is the exact induced current produced by the exact dielectric profile $\overline{\zeta}$. However, since the exact electrical parameter and the induced current are not available, the Born approximation used in VBIM approximates the exact induced current $\overline{J}$ using $\overline{J}_{k-1}$ generated by ζ_{k-1}. S-VBIM approximates the exact induced current $\overline{J}$ by $\overline{J}_{k-1} + \delta\overline{J}^d$, where $\delta\overline{J}^d$ is the deterministic part of the variational induced current $\delta\overline{J}$. Hence, the total electric field is:

$$\overline{E}^{tot} = \overline{E}^{inc} + \overline{G}_D \cdot \left(\overline{J}_{k-1} + \delta\overline{J}^d\right) \tag{12}$$

S-VBIM is reported to have a faster convergence speed than VBIM [21]. The cost function for the S-VBIM is defined as

$$f(\delta\zeta) = \frac{\left\|\delta\overline{E}^{scat} - \overline{G}_s \cdot \delta\zeta \cdot \overline{E}^{tot}\right\|^2}{\left\|\overline{E}^{scat}\right\|^2} + \frac{\left\|\delta\zeta \cdot \overline{E}^{tot}\right\|}{\left\|\delta\overline{J}^d\right\|^2} \tag{13}$$

In this cost function, the only regularization term is L. As L has an integer value and is not larger than L_0, it is more convenient than finding a proper regularization parameter in a large range in Tikhonov regularization.

In order to alleviate the nonlinearity and ill-posedness of quantitative MWI based ISPs, many nonlinear iterative inversion methods have been proposed [19–24]. However, they usually consume large number of computational resources. The iterative procedure is complex and time-consuming to arrive at the final solution. Hence, real-time imaging is not feasible in the case of such iterative methods. On the other hand, deep learning techniques can be tested in a single step, paving way for the imaging of real-time scenarios. Therefore, a learning-based inversion method which uses U-net is proposed in this work to efficiently realize quantitative MWI.

2.3. Inversion Using Deep Learning-Based Methods

Usually linear optimization techniques are used to solve the ill-posed problem. For each iteration step, an updated dielectric profile is estimated from the previous profile, and it repeats progressively until a better estimate of the dielectric profile is obtained. In this paper, a Convolutional Neural Network (CNN) is employed to solve the inverse ill-posed problem. Here the goal is not to imitate iterative methods, but rather to explore a state of art CNN architecture for solving such an ill-posed problem. The proposed architecture of CNN is based on the U-net which is generally used for the purpose of image segmentation [25]. Recent works published in this area [26, 27] show that the U-net CNN architecture is well suited for solving ISP along with Back-propagation, Contrast source inversion, etc.

Figure 3 shows the inputs given to the CNN used for solving the inverse scattering problem. The U-net architecture consists of two paths [15], one contracting path and an expansive path in the form of **U** in the English alphabet. The contracting path (left side) consists of repeated application of 3×3 convolutions, batch normalization, Rectified Linear Unit (ReLU), and a 2×2 max pooling operation. The expansive path proceeds in the reverse direction to arrive at the final reconstructed profile.

In this paper, the initial contrast function (real and imaginary) retrieved by solving SVBIM is directly taken as the inputs to the U-net and the contrasts ζ on imaging domain, and V is used as the target for the network. During the contraction path, the spatial information decreases, while the feature
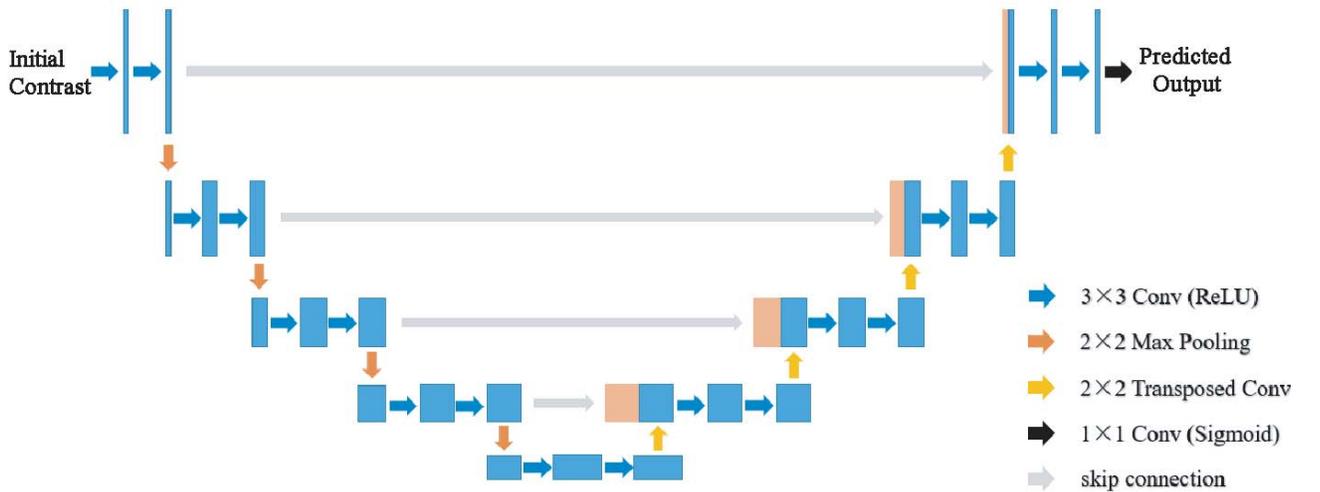

Figure 3. U-net architecture for quantitative reconstruction.

information increases during the expansion path. The features and spatial information are combined through a 3×3 up-convolution within the U-net architecture. It ensures the one-to-one corresponding relationship between the input and output in the training, and the trained U-net can realize quantitative MWI. Since the results obtained from SVBIM are complex values, the input and output channel number of the original U-Net is modified, and a 2-channel U-net is adopted.

3. SIMULATION AND EXPERIMENTAL RESULTS

This section presents the simulated and experimental reconstruction results. RMSE is used as the metric for measuring the quality of the reconstructed profile which is defined by [28]

$$RMSE = \sqrt{\frac{1}{M} \sum_m \sum_n \left| \frac{\epsilon_{r;m,n}^r - \epsilon_{r;m,n}^t}{\epsilon_{r;m,n}^t} \right|^2} \tag{14}$$

where $\epsilon_{r;m,n}^r$ & $\epsilon_{r;m,n}^t$ represent the reconstructed and true dielectric permittivities of the object profile ($m = 1, 2, \ldots, M_1$; $n = 1, 2, \ldots, M_2$; $M = M_1 \times M_2$ is the total number of square cells).

3.1. Training and Testing of U-Net

For the proposed technique, MNIST database of handwritten digits [30] from 0–9 is chosen for the training and testing. Each image from the database is considered to be an object domain, and the physical size of the image is set to $10\lambda \times 10\lambda$, which is discretized into 32×32 grids. The background medium is assumed to be air with $\epsilon_B = 1$. Generally, antennas are arranged around the object at a distance greater than 10 times of the wavelength. In the simulation model, both transmitting and receiving antennas are assumed to be arranged in a circular manner of radius 12λ ($1.2\,\text{m}$) from the center of the object domain. A set of 16 transmitter antennas are used to excite the object, and a set of 32 receiver antennas are assumed to collect the back scattered signal which are evenly distributed between 0 and 360 degrees (0 degrees included). The object is excited by incident plane waves with a Gaussian pulse of frequency $3\,\text{GHz}$. In a real-time scenario, random events such as discrete nature of radiation, variation in detector sensitivity, faults in the measuring device, environmental errors (due to factors like stray magnetic fields, vibration, etc.), and errors introduced by the experimenter are always present, and hence, its effect has to be considered. Usually an additive Gaussian noise is added to simulate such kinds of noise, and hence a $30\,\text{dB}$ additive white Gaussian noise (AWGN) has been added [31] to the scattered data before inverse profiling. A scattering matrix having a size of $N_t \times N_r$ is composed from the scattered data. This matrix is used for finding the initial object profile using SVBIM (described in the Section 2.1). This profile data which consist of complex dielectric values can be used as the input training vector for a U-net.

From the MNIST training database, a set of randomly chosen 5000 images are used for training the U-net, where 4000 images are used for the training and 1000 for testing the U-net. The coarsely reconstructed image corresponding to each image in the database obtained after solving the S-VBIM (initial contrast profile) is used as the input for training the U-net. The actual profiles are considered as the outputs from the network. The sizes of input and output images of the Unet are both $N \times N \times 2$, comprising the real and imaginary parts of the contrast. The real part of the reconstructed final profile is generally reported in literature [28]. *An adaptive moment estimation (Adam) optimizer is chosen to optimize the half-mean-squared-error loss function in Equation 15, with batch size of 32, epoch setting as 100, and the learning rate of 10^{-4}.* In order to reduce over-fitting, regularization technique available for optimization of the deep neural network which is called as 'dropout' is set at 0.2 [29].

$$hmser = \frac{1}{2} \sum_{i=1}^{m} \left(h_\theta \left(x^i \right) - \left(x^i \right) \right)^2 \tag{15}$$

For testing the trained network, random images from MNIST testing database are used as the input to the Unet. The digit-like object profiles shown in Figs. 4(a)–(c) are considered lossless having dielectric value of $\epsilon_r = 3$. Figs. 4(d)–(e) show the corresponding reconstructed profiles. An image
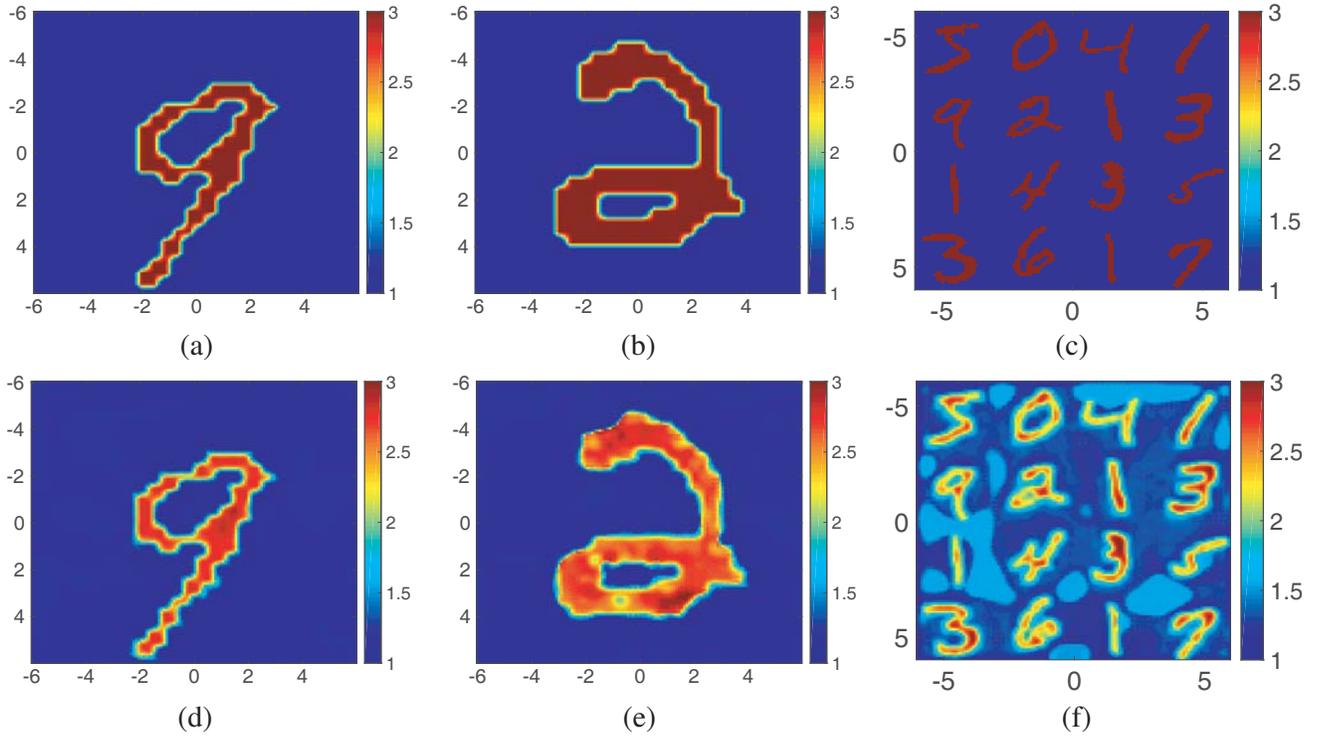
Figure 4. Reconstruction of digit-like objects with relative permittivity $\epsilon_r=3$.

composed of a group of 16 characters is tested along with the individual dataset. The Fig. 4(f) shows the reconstructed profile for the combined image.

In order to validate the overall ability of the trained network, the performance of the proposed method is compared to [17] using the 'Austria profile' (Fig. 5(a)).

The Austria profile has a different shape compared with the MNIST database. This profile consists of two disks and a ring [21]. The background is assumed to be air, and the dielectric value for the profile is assumed to be 3. The measured scattered fields are obtained by solving the forward problem using MoM with discretization of 100×100. In order to have a real-time scenario, an additive Gaussian noise of 30 dB is added along with the simulated scattered field before the inversion process. Fig. 5(b) shows the reconstructed Austria profile using the trained network. Table 1 shows the RMSE values of the proposed method in comparison with BP and BP-DSM techniques. The error values demonstrate better accuracy of the proposed method than the two methods BP and BP-DSM.
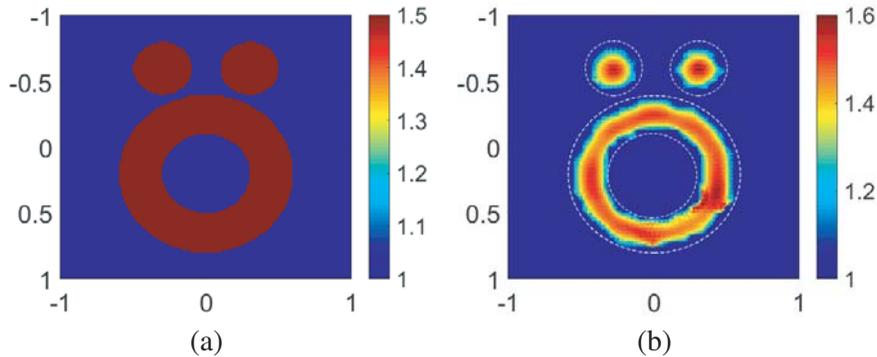

Figure 5. Reconstruction Austria profile. (a) Ground Truth. (b) Reconstructed profile.

Table 1. RMSE values for the reconstructed Austria Profile.

Target	Reconstruction Errors
BP [17] 2020	0.1278
BP-DSM [17] 2020	0.1070
Proposed	0.0813

All computations are performed in a small-scale server with the configuration of 32 GB access memory, Intel Xeon E5-1620v2 central processing unit, NVIDIA GeForce GTX 1050Ti. Deep Learning network part was designed using Tensorflow libraries, and the SVBIM algorithm was implemented using MATLAB 2017.

3.2. Experimental Results

In this section, the proposed technique is validated experimentally using "FoamDielExt" experimental data from 2 GHz to 10 GHz provided by the Institute Fresnel, Marseille, France [18]. The setup used for imaging consists of a fixed foam cylinder and a plastic cylinder located outside the foam as shown in Fig. 6. This profile consists of two scattering cylinders, where the yellow object is a dielectric (plastic) with a relative permittivity of 3 ± 0.3, and the blue object is a dielectric (foam) with a relative permittivity of 1.45 ± 0.15, having diameters of 3.1 cm & 8 cm, respectively. For the inversion of experimental data, an additional training data set of synthetic images are embedded along with the current MNIST database. For each synthetic image, two circles are generated at random location and size. The larger circle has a lower dielectric value compared with the smaller circle. The relative permittivity of two circles is chosen in the range of $[1.3, 3.5]$. All the scattered values measured from each synthetic profile are added with an additive white Gaussian noise corresponding to 30 dB of input SNR. This combined data set and their forward scattering data are used for training the CNN. The network is trained for 1000 epochs to minimize the RMSE between the input and output profiles.

The reconstruction results at 4 GHz are shown in the Fig. 6. For a fair comparison, imaging domain is discretised into a mesh grid of size 32×32, and the results obtained by the proposed method are compared with the learning based hybrid method [17]. Table 2 shows the RMSE value evaluated for the proposed method and the method reported in [17]. It can be noted that the proposed method has a maximum reduction in noise as compared with the hybrid method, with an RMSE value of only 0.1037 against 0.1631.
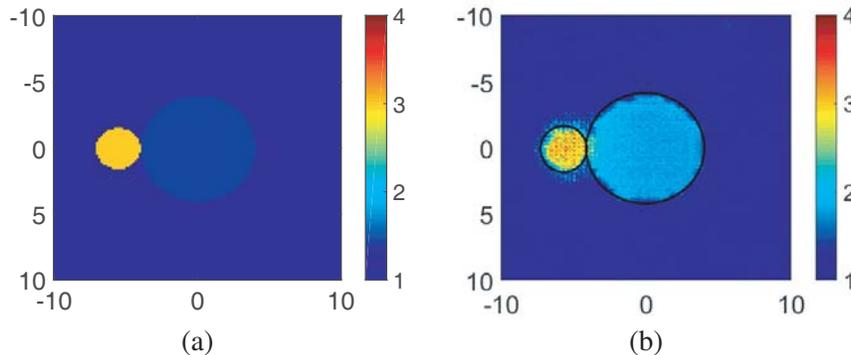

Figure 6. Reconstruction of $FoamDielExt^{TM}$ database by the proposed method. (a) Actual Profile. (b) Reconstructed Profile.

In this paper, SVBIM is used for generating the initial contrast function. SVBIM method uses Singular Value decomposition wherein the smaller singular values are truncated resulting in better robustness against noise. Hence, the initial contrast profile is better than [17]. Moreover, the network

Table 2. RMSE results for the reconstructions in Fig. 6.

Target	Reconstruction Errors
BP [17] 2020	0.1858
BP-DSM [17] 2020	0.1631
Proposed	0.1037

used for training purpose has two channels, with each channel designed to handle both real and imaginary parts of the initial contrast profile, obtained through SVBIM, whereas [17] uses only a single channel to handle the real valued initial contrast profile.

4. CONCLUSION

In this paper, a two-step process employing the deep learning approach is proposed to solve a full-wave inverse scattering problem, which is aimed for the quantitative reconstruction of the dielectric permittivities from the measured scattered field. Initially, the contrast function is reconstructed using S-VBIM, and this initial profile is fed to a trained U-net to reconstruct the dielectric permittivities of the scatterer. The capability of the proposed method is clearly observed from the results of numerical analysis as well as experimental validation. By comparing with similar deep learning methods like BP-DSM, it is found that the RMSE obtained by the proposed method is 0.1037 against 0.1631.

REFERENCES

1. Chandra, R., H. Zhou, I. Balasingham, and R. M. Narayanan, "On the opportunities and challenges in microwave medical sensing and imaging," *IEEE Transactions on Biomedical Engineering*, Vol. 62, No. 7, 1667–1682, 2015.
2. Ambrosanio, M., P. Kosmas, and V. Pascazio, "A multithreshold iterative DBIM-based algorithm for the imaging of heterogeneous breast tissues," *IEEE Transactions on Biomedical Engineering*, Vol. 66, No. 2, 509–520, 2018.
3. Chen, X., *Computational Methods for Electromagnetic Inverse Scattering*, Wiley, Hoboken, NJ, USA, 2018.
4. Randazzo, A., C. Ponti, A. Fedeli, C. Estatico, P. D'Atanasio, M. Pastorino, and G. Schettini, "A two-step inverse-scattering technique in variable-exponent lebesgue spaces for through-the-wall microwave imaging: Experimental results," *IEEE Transactions on Geoscience and Remote Sensing*, 2021.
5. Huang, T. and A. S. Mohan, "Microwave imaging of perfect electrically conducting cylinder by micro-genetic algorithm," *IEEE Antennas and Propagation Society Symposium*, Vol. 1, IEEE, 2004.
6. Semenov, S. Y., et al., "Microwave-tomographic imaging of the high dielectric-contrast objects using different image-reconstruction approaches," *IEEE Trans. Microw. Theory Tech.*, Vol. 53, No. 7, 2284–2294, Jul. 2005.
7. Rajan, S. D. and G. V. Frisk, "A comparison between the Born and Rytov approximations for the inverse backscattering problem," *Geophysics*, Vol. 54, 864–871, 1989.
8. Majobi, P. and J. LeVetri, "Comparison of TE and TM inversions in the framework of the Gauss-Newton Method," *IEEE Transactions on Antennas and Propagation*, Vol. 64, 1336–1348, 2010.
9. Rocca, P., M. Benedetti, M. Donelli, D. Franceschini, and A. Massa, "Evolutionary optimization as applied to inverse problems," *Inverse Probl.*, Vol. 25, 1–41, 2009.
10. Candès, E. J. and M. B. Wakin, "An introduction to compressive sampling," *IEEE Signal Processing Magazine*, Vol. 25, No. 2, 21–30, 2008.
11. Lustig, M., D. Donoho, and J. M. Pauly, "Sparse MRI: The application of compressed sensing for rapid MR imaging," *Magnetic Resonance in Medicine*, Vol. 58, No. 6, 1182–1195, 2008.

12. Pan, X. and E. Y. Sidky, "Image reconstruction in circular cone-beam computed tomography by constrained, total-variation minimization," *Physics in Medicine and Biology*, Vol. 53, No. 17, 4777–4807, 2008.

13. Naghsh, N. Z., A. Ghorbani, and H. Amindavar, "Compressive sensing for microwave breast cancer imaging," *IET Signal Processing*, Vol. 12, No. 2, 242–246, 2017.

14. Rekanos, I. T., "Neural-network-based inverse-scattering technique for online microwave medical imaging," *IEEE Transactions on Magnetics*, Vol. 38, No. 2, 1061–1064, 2002.

15. Wei, Z. and X. Chen, "Deep-learning schemes for full-wave nonlinear inverse scattering problems," *IEEE Transactions on Geoscience and Remote Sensing*, Vol. 57, No. 4, 1849–1860, 2019.

16. Guo, R., X. Song, M. Li, F. Yang, S. Xu, and A. Abubakar, "Supervised descent learning technique for 2-D microwave imaging," *IEEE Transactions on Antennas and Propagation*, Vol. 67, No. 5, 3550–3554, 2019.

17. Zhang, L., K. Xu, R. Song, X. Z. Ye, G. Wang, and X. Chen, "Learning-based quantitative microwave imaging with a hybrid input scheme," *IEEE Sensors Journal*, Vol. 20, No. 24, 15007–15013, 2020.

18. Geffrin, J.-M., P. Sabouroux, and C. Eyraoud, "Free space experimental scattering database continuation: Experimental set-up and measurement precision," *Inverse Probl.*, Vol. 21, No. 6, 117–130, 2005.

19. Chew, W. C. and Y. M. Wang, "Reconstruction of two-dimensional permittivity distribution using the distorted Born iterative method," *IEEE Trans. Medical. Imag.*, Vol. 9, No. 2, 218–225, 1990.

20. Anzengruber, S. W. and R. Ramlau, "Convergence rates for morozov's discrepancy principle using variational inequalities," *Inverse Problems*, Vol. 27, No. 10, 105007, 2011.

21. Liu, Z. and Z. Nie, "Subspace-based variational born iterative method for solving inverse scattering problems," *IEEE Geoscience and Remote Sensing Letters*, Vol. 16, No. 7, 1017–1020, Jul. 2019.

22. Li, M., O. Semerci, and A. Abubakar, "A contrast source inversion method in the wavelet domain," *Inverse Probl.*, Vol. 29, No. 2, 025015, 2013.

23. Ye, X., X. Chen, Y. Zhong, and K. Agarwal, "Subspace-based optimization method for reconstructing perfectly electric conductors," *Progress In Electromagnetic Research*, Vol. 100, 119–128, 2010.

24. Zhong, Y. and X. Chen, "An FFT twofold subspace-based optimization method for solving electromagnetic inverse scattering problems," *IEEE Transactions on Antennas and Propagation*, Vol. 59, No. 3, 914–927, 2011.

25. Ronneberger, O., P. Fischer, and T. Brox, "U-net: Convolutional networks for biomedical image segmentation," *Proc. 18th Int. Conf. Med. Image Comput. Comput.-Assist. Intervention*, 234–241, 2015.

26. Yao, H. M., W. E. I. Sha, and L. Jiang, "Two-step enhanced deep learning approach for electromagnetic inverse scattering problems," *IEEE Antennas and Wireless Propagation Letters*, Vol. 18, No. 11, 2254–2258, Nov. 2019.

27. Xu, K., L. Wu, X. Ye, and X. Chen, "Deep learning-based inversion methods for solving inverse scattering problems with phaseless data," *IEEE Transactions on Antennas and Propagation*, Vol. 68, No. 11, 7457–7470, 2020.

28. Zhang, Z., "Improved adam optimizer for deep neural networks," *2018 IEEE/ACM 26th International Symposium on Quality of Service (IWQoS)*, 1–2, Banff, AB, Canada, 2018.

29. Rahangdale, A. and S. Raut, "Deep neural network regularization for feature selection in learning-to-rank," *IEEE Access*, Vol. 7, 53988–54006, 2019.

30. Deng, L., "The MNIST database of handwritten digit images for machine learning research [Best of the Web]," *IEEE Signal Processing Magazine*, Vol. 29, No. 6, 141–142, Nov. 2012.

31. Azghani, M. and F. Marvasti, "L2-regularized iterative weighted algorithm for inverse scattering," *IEEE Transactions on Antennas and Propagation*, Vol. 64, No. 6, 2293–2300, 2016.